Mechanisms and consequences of horizontal gene transfer in cell wall-deficient cells of Kitasatospora viridifaciens

Kapteijn, R.

Chapter 4.

Endocytosis-like DNA uptake by cell wall-deficient bacteria

Renée Kapteijn, Shraddha Shitut, Dennis Aschmann, Le Zhang, Marit de Beer, Deniz Daviran, Rona Roverts, Anat Akiva, Gilles P. van Wezel, Alexander Kros and Dennis Claessen

The data presented in this chapter is published as part of:

Kapteijn, R., Shitut, S., Aschmann, D., Zhang, L., de Beer, M., Daviran, D., Roverts, R., Akiva, A., van Wezel, G. P., Kros, A., & Claessen, D. Endocytosis-like DNA uptake by cell wall-deficient bacteria. *Nat Commun* **13**, 5524 (2022).

Abstract

Endocytosis is an uptake mechanism commonly assumed to be restricted to eukaryotic cells. Here, we report that an endocytosis-like process can take place in permanently cell wall-deficient cells of the filamentous actinobacterium *Kitasatospora viridifaciens*. L-form cells engulf DNA and other extracellular material via invagination of the cytoplasmic membrane, leading to formation of intracellular vesicles. Specifically, we show that L-forms can take up plasmid DNA, polysaccharides (dextran) and 150-nm lipid nanoparticles. Uptake is inhibited by sodium azide or incubation at 4 °C, suggesting the process is energy-dependent. The encapsulated materials are released into the cytoplasm upon degradation of the vesicle membrane. This provides a mechanism by which L-forms are transformed upon incubation with plasmid DNA, without the use of polyethylene glycol (PEG). Given that cell wall-deficient bacteria are considered a model for early life forms, our work reveals a possible mechanism for primordial cells to acquire food or genetic material before invention of the bacterial cell wall.

Introduction

A unifying trait for all cellular life forms is the encapsulation of cellular contents by a cell membrane. This dynamic bilayer is composed of a variety of lipids such as phospholipids and cholesterol. It serves as an anchor point for the localization of proteins [285, 286] and has a barrier function to regulate the entry of compounds into the cytoplasm. Whereas some molecules such as water and oxygen can passively diffuse across this layer, other compounds require transport proteins or enter the cell via a process called endocytosis [287, 288]. Endocytosis is a mechanism by which fluids, molecules, cell membrane components and even entire viruses and bacteria are internalized [289]. During this process, the cell membrane bulges inwards and entraps extracellular cargo inside a vesicle in the cell. Depending on the cargo, different endocytic pathways are in place to ensure the correct processing inside the cell, leading to degradation within lysosomes or recycling to the cell surface [290, 291].

Endocytosis is generally thought to be restricted to eukaryotes [292]. A few endocytosis-like features have been reported in prokaryotes, such as for the magnetotactic bacterium *Magnetospirillum magneticum* whereby magnetite crystals are contained in cell membrane invaginations [293], and for the planctomycete '*Candidatus* Uab amorphum' which engulfs bacteria and small eukaryotic cells as a source of food [294]. In addition, the putative uptake of fluorescently-labelled probes into intracellular 'vacuoles' was observed for *Bacillus subtilis* undergoing a cell wall-deficient L-form state [92]. Unlike the vast majority of bacteria, L-form bacteria are not enclosed by a protective cell wall, and proliferate indefinitely via biophysical processes [88, 95, 102, 103]. L-form proliferation has striking similarities to the shape changes observed during reproduction of giant lipid vesicles which is driven by physicochemical membrane dynamics [93]. Their primitive cell-like characteristics make L-forms an attractive model system to study the evolution of early life [93, 94].

Previous research shows that an L-form of the filamentous actinobacterium *Kitasatospora viridifaciens* has the ability to take up extracellular plasmid DNA, leading to transformation (Chapter 3). In addition, preliminary work shows that L-forms of *Listeria monocytogenes* can take up plasmid DNA and produce the plasmid-encoded cyan fluorescent protein [258]. These transformation evens did not rely on use of polyethylene glycol (PEG), a compound widely used to transform wall-less cells such as protoplasts [223]. Additionally, DNA uptake in the *K. viridifaciens* L-form was not dependent on proteins homologous to proteins required for natural transformation in other bacterial species, and *L. monocytogenes* does not contain a functional competence system [258], suggesting that a different uptake mechanism is utilized. Interestingly, specific mammalian cells can take up DNA, which is followed by active expression of reporter genes [260]. This was proposed to occur via endocytosis, although the exact mechanism is unclear [259]. We therefore hypothesize that an endocytosis-like mechanism could be responsible for DNA uptake in L-form cells.

In this work, we show that DNA uptake by L-forms of *K. viridifaciens* is facilitated by a mechanism akin to eukaryotic endocytosis, involving the invagination of the cell membrane leading to internal vesicle formation. Furthermore, we show that this mechanism allows the non-specific uptake of other macromolecules from the environment as well. Given that L-forms are considered a model for early cellular life, our work provides insight into how ancient cells may have acquired large biomolecules from the environment without the need for complex transport machineries.

Results

Internal vesicle formation in L-forms results in DNA uptake

We previously showed that L-forms of *K. viridifaciens* can naturally take up extracellular DNA without relying on genes that encode proteins with homology to canonical DNA-uptake machinery (Chapter 3). To investigate the mechanism facilitating DNA uptake, we added Cy5-labelled plasmid DNA to L-forms expressing cytoplasmic eGFP. After 72 h incubation, labelled plasmid DNA was found either on the outside of the L-form cell membrane, or within an apparent internal vesicle (Fig. 1A, Supplementary Movie 1, and Supplementary Fig. 1A). As the internal vesicles were devoid of eGFP, we reasoned that they could have originated by an invagination process of the membrane, whereby extracellular material becomes trapped inside the vesicles. To test this directly, we incubated eGFP-expressing L-forms with the fluorescent dye SynapseRed C2M (SynapseRed). Given that styryl dyes, such as SynapseRed (equivalent to FM5-95), cannot diffuse through cell membranes [295, 296], any fluorescent signal on the membranes surrounding internal vesicles would be a strong argument that such vesicles were derived from the cell membrane. Indeed, SynapseRed was found to not only stain the cell membrane of the L-forms but also the membranes of internal vesicles after overnight incubation (Fig. 1B). Staining with SYTO 9 further indicated that chromosomal DNA was present in the cytoplasm but not inside internal vesicles (Fig. 1C).

Next to permanently wall-less L-form cells, *K. viridifaciens* can produce temporary wall-deficient cells called S-cells (stress-induced cells) from the tip of the hyphae. S-cells are formed upon growth of *K. viridifaciens* under high osmotic pressure, and can revert back to a walled state under specific conditions [15]. Wall-less cells can also be generated artificially from walled bacterial cells using lysozyme, thereby generating protoplasts [223]. Previous work (Chapter 3) showed that only L-form cells could consistently take up external DNA, but the temporary wall-less protoplasts or S-cells could not. Incubation of protoplasts producing cytoplasmic eGFP with SynapseRed showed that areas with less cytoplasmic eGFP fluorescence were caused by the presence of internal membrane structures rather than by formation of internal vesicles (Fig. 1D). Similar incubation of S-cells showed the presence of internal vesicle-like structures devoid of cytoplasmic eGFP. However, unlike for L-forms,

subsequent staining of S-cells that produce cytoplasmic mCherry with SYTO 9 indicated that these dark regions were filled with chromosomal DNA (Fig. 1D). As SynapseRed is a membrane-impermeable dye, the staining of membrane structures in S-cells may reflect enhanced membrane permeability instead of staining due to the invagination of the cell membrane. To test the diffusion of the dye across the cell membrane, L-forms and S-cells were incubated with SynapseRed at 30 °C and at 4 °C to enable and prevent possible membrane invagination, respectively. Whereas internal membrane was stained in S-cells both at 30 °C and 4 °C, this was only observed at 30 °C for L-forms (Supplementary Fig. 1B). This suggests that the staining of a membrane in S-cells by SynapseRed is due to permeability of the cell membrane for the dye, in contrast to L-forms, in which staining is a result of invagination of the cell membrane.

To compare the presence of putative internal vesicle structures in the different cell types, the percentage of L-forms, protoplasts and S-cells with these structures was quantified. Cells producing cytoplasmic mCherry (*alpha* pRed* or S-cells and protoplasts derived from *K. viridifaciens* pRed*) were stained with SynapseRed and imaged directly or incubated for 72 h to stain membranes. DNA was visualized with SYTO 9 before imaging. The number of cells with regions lacking fluorescence emission from the cytoplasm, DNA, and membrane, which could indicate the presence of internal vesicles, was quantified (Supplementary Table 1). Using this method, L-forms were observed to have around 6- to 11-fold higher occurrence of such regions than S-cells (L-forms: 24.5 and 14.7%; S-cells: 2.2 and 2.6% after direct imaging or 72 h incubation, respectively), and putative vesicles were rarely observed for protoplasts (<0.5%). If these regions in S-cells and protoplasts would be actual internal vesicles, their occurrence is likely not sufficient to detect consistent transformation with DNA. Taken together, these results strongly suggest that the observed vesicles inside L-forms originate from the invagination of the cell membrane whereby extracellular DNA may become trapped inside such vesicles, whereas this is not evident for S-cells and protoplasts.

L-forms take up extracellular material via an endocytosis-like mechanism

In eukaryotes, endocytosis is a process that enables the uptake of external cargo via internal vesicle formation, which is eventually degraded or recycled [289, 297]. Fluorescently labelled dextrans are widely used as markers for endocytosis in eukaryotes as they cannot pass the cell membrane [298, 299]. To identify if such an endocytosis-like process could be present in L-forms and to visualize the uptake of external materials, we incubated the cells with Dextran-Texas Red (D-TR) and performed timelapse imaging. The L-form strain used (*alpha* pKR2) also expresses DivIVA-eGFP, which has a strong affinity for negatively curved membrane regions [300]. Such regions are expected to be formed upon the invagination of the membrane. After 290 min of incubation, D-TR was visible inside the L-form and faint spots of DivIVA-eGFP started to appear adjacent to this region (Fig. 1E and Supplementary Movie 2). This progressed to a

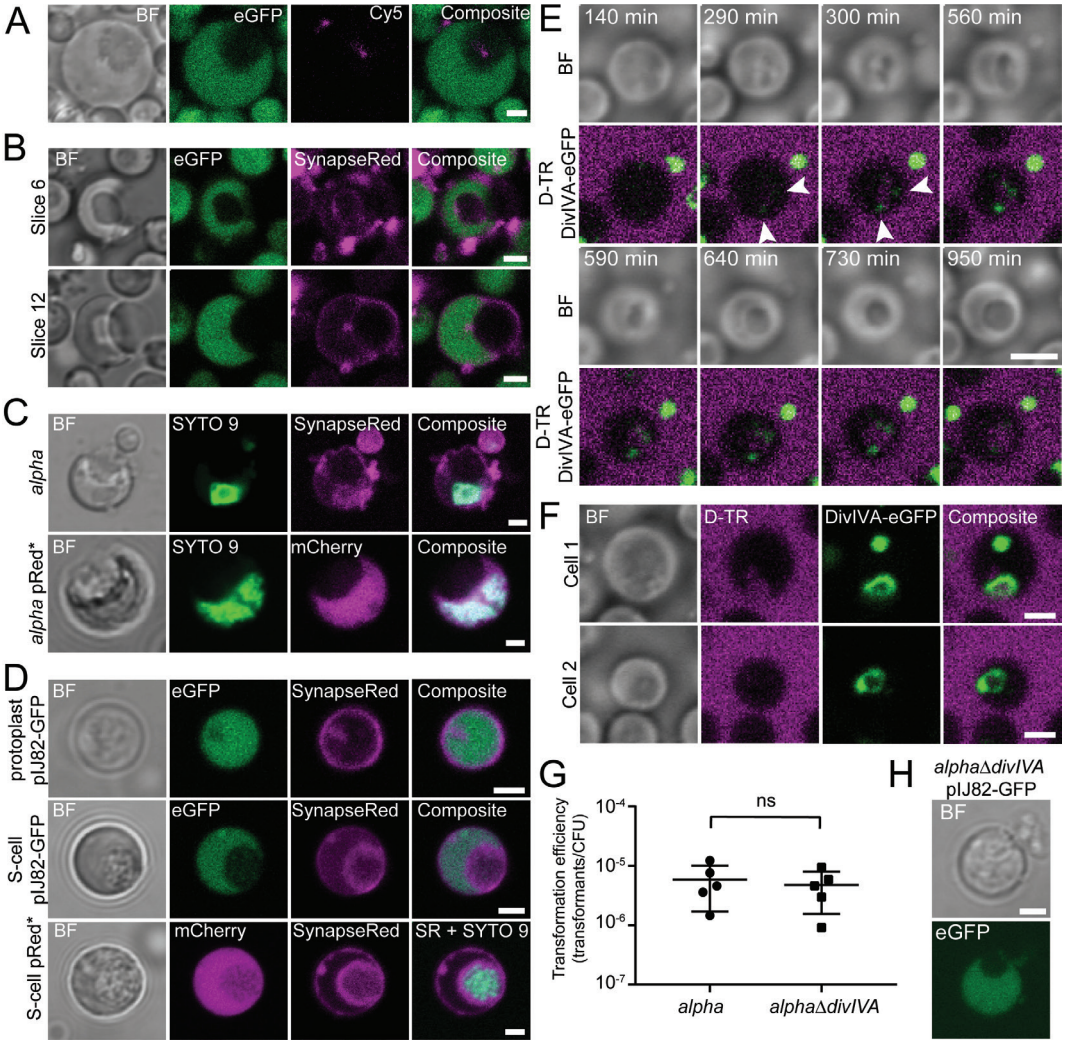

Figure 1. Formation of internal vesicles and uptake of extracellular material in L-forms

(A) Representative fluorescence micrograph of *alpha* pIJ82-GFP (cytoplasmic eGFP; green) incubated with Cy5-labelled plasmid DNA (pFL-*ssgB*; magenta) for 72 h (n = 3 observations from one experiment). BF = brightfield. See also Supplementary Movie 1. **(B)** Incubation of *alpha* pIJ82-GFP after overnight incubation with the membrane-impermeable dye SynapseRed C2M (SynapseRed; magenta), showing two z-slices at different heights of one L-form cell. A representative micrograph of six observations from one experiment is shown. **(C)** Representative micrograph of *alpha* (n = 7 observations from one incubation) and *alpha* pRed* (n = 9 observations from one incubation) stained with SYTO 9 (green) to indicate chromosomal DNA. L-form *alpha* is stained with SynapseRed C2M (SynapseRed; magenta) to visualize cell membranes, whereas (absence of) cytoplasmic mCherry for *alpha* pRed* (magenta) indicates the presence of an internal vesicle. Cells were imaged directly after addition of the fluorescent dyes. **(D)** Representative images of protoplasts and S-cells of *K. viridifaciens* pIJ82-GFP producing cytoplasmic eGFP incubated with SynapseRed (SR) for 72 h (top rows, at least six observations from two independent experiments with S-cells and protoplasts), and S-cells of *K. viridifaciens* pRed* producing cytoplasmic mCherry incubated with SynapseRed and SYTO 9 for 72 h (bottom row, three observations from one experiment). Note that the presence of internal membrane structures and/or DNA can cause a reduction in cytoplasmic fluorescence emission. **(E)** Stills of a 950-min timelapse imaging experiment of *alpha* producing DivIVA-eGFP (*alpha* pKR2) (green) incubated

with 3 kDa Dextran-Texas Red (D-TR; magenta) (n = 1). Arrows indicate localization of DivIVA-eGFP. See also Supplementary Movie 2. **(F)** Representative micrographs of the formation of foci and ring-structures of DivIVA-eGFP in *alpha* pKR2 (green) after overnight incubation with D-TR (magenta) (more than 50 observations from one experiment). Note that L-forms are able to take up fluorescently stained DNA and dextran by formation of internal vesicles. **(G)** Transformation efficiency of 168 h *alpha* and *alpha*Δ*divIVA* using pFL-*ssgB*. ns: not significant (two-sided independent t-test, $t(8)$=0.489, P = 0.638). CFU = colony forming units. Data are represented as mean ± SD with individual data points, n = 5 biological replicates. **(H)** L-forms without DivIVA can produce internal vesicles as shown for 120 h *alpha*Δ*divIVA* pIJ82-GFP producing cytoplasmic eGFP (n = 2 observations from one culture). Scale bars indicate 2 μm.

clear inward bulging of the cell membrane with two foci of DivIVA-eGFP on either side of the invaginated membrane and an inflow of D-TR (t = 560 min). After 640 min an internal vesicle was formed that contained D-TR. In other cells, DivIVA-eGFP appeared to form a ring-like structure, which sometimes enveloped the invaginating membrane (Fig. 1F cell 1 and 2). The presence of DivIVA near the site of invagination implies the presence of negatively curved regions in the membrane. Notably, DivIVA is not required for vesicle formation or DNA uptake, as the deletion of *divIVA* (*alpha*Δ*divIVA*) had no effect on transformation (two-sided independent t-test, $t(8) = 0.489$, $P = 0.638$) (Fig. 1G), and internal vesicles were still formed by this strain (Fig. 1H). Furthermore, internalization of D-TR was also observed in L-forms that did not express DivIVA-eGFP, indicating that uptake is not a consequence of the presence of the fusion protein (Supplementary Fig. 1C).

Incubation of protoplasts and S-cells with D-TR up to 72 h did not result in clear D-TR encapsulation in internal vesicles (Supplementary Fig. 1D). To quantify this, cells producing cytoplasmic eGFP were incubated with D-TR or PBS for 72 h. The percentage of cells with regions lacking eGFP but containing D-TR in this region was counted. Repeated incubation (in duplo) resulted in uptake of D-TR in around 6% of L-form cells and no uptake for the control with PBS (Supplementary Table 2). No clear uptake was observed for S-cells and protoplasts incubated with D-TR when compared to control cells incubated with PBS (S-cells: 0.9 and 1.7% with D-TR versus 0 and 2.1% with PBS; protoplasts: 0 and 1.1% with D-TR versus 0 and 0.8% with PBS). Altogether, these results show that the invagination of the cell membrane of L-forms can lead to internal vesicle formation and may represent an endocytosis-like mechanism allowing uptake of molecules, including DNA, from the environment.

Lipid nanoparticles are internalized via vesicle formation in an energy-dependent manner

Lipid nanoparticles (LNPs) are non-viral particles that are used to deliver nucleic acids and drugs to human cells via endocytosis [301]. LNPs do not have a lipid bilayer structure, but consist of an electron-dense, hydrophobic core of lipids that encapsulate nucleic acids by electrostatic interactions and are surrounded by a layer of PEG-lipids [301]. Internalized LNPs

are located in endosomes, which are membrane-bound organelles of the endocytic pathway. Subsequent acidification causes the ionizable lipids of the LNPs to become positively charged, which allows the LNP to destabilize the endosomal membrane and deliver its cargo into the cell. LNPs can also be fluorescently tagged by the incorporation of fluorophore-conjugated phospholipids. To further explore the ability of L-forms to take up large external particles, the cells were incubated with rhodamine-labelled LNPs (LNP-LR, containing 18:1 Liss Rhod PE) with an average size of 150 nm, to allow their detection inside L-forms. After addition of LNP-LR to 168 h L-forms, a clear fluorescent signal, likely generated by multiple LNP particles, could be detected inside cells after overnight incubation, as well as localization of LNPs to the cell membrane (Fig. 2A and Supplementary Fig. 2A, B). When L-forms were used that produced eGFP in the cytoplasm, vesicles only contained LNPs and not eGFP, strongly suggesting that the LNPs had been internalized in vesicles devoid of the cytoplasm (Fig. 2B, C and imaging control Supplementary Fig. 2C).

Importantly, the addition of the metabolic inhibitor sodium azide (1 mM, 2.5 mM, or 10 mM), which targets the respiratory chain [302], or incubation of cells at 4 °C affected the localization of LNP-LR (Fig. 2D, E, Supplementary Fig. 2D, E and Supplementary Fig. 3). These conditions are commonly used to inhibit endocytosis by repressing energy production [303, 304]. Under such conditions, the LNPs appeared to localize to the cell membrane rather than inside the cell. The inhibiting effect of sodium azide and incubation at 4 °C on uptake of extracellular material by L-forms was quantified using D-TR, as capturing the uptake of LNP-LR was too infrequent to quantify accurately. Strikingly, a significant reduction of D-TR uptake by L-forms was observed in the presence of 2.5 mM sodium azide (5.9% versus 1.9% of cells showing D-TR uptake for control and sodium azide, respectively; two-proportion z-test, $z = 3.111$, one-sided $P < 0.001$), and incubation of L-forms at 4 °C completely inhibited D-TR uptake (Fig. 2F). These results are consistent with an uptake process in L-forms that is energy-dependent, whereby external material is internalized by a membrane invagination process.

High-resolution imaging of L-forms using cryo-FIB-SEM

To better understand the ultrastructure and composition of intracellular vesicles, L-forms were imaged using 3D cryo-correlative light and electron microscopy (cryo-CLEM) (Fig. 3A). Cryo-FIB-SEM (focused ion beam–scanning electron microscopy) allows the 3D high-resolution imaging of L-forms and internal vesicles. The cryogenic sample preparation and imaging ensure that the L-forms are visualized in a near-to-native state via rapid freezing under high-pressure conditions that allow the transformation of liquid to amorphous ice [305-307]. Following high-pressure freezing, cells with putative intracellular vesicles were detected based on internal darker regions lacking cytoplasmic eGFP using *alpha* pIJ82-GFP (Supplementary Fig. 4). Specific L-forms (example of selection in Fig. 3B, C) were imaged in detail using cryo-FIB-SEM. The reduction in cytoplasmic eGFP indeed matched the presence of internal

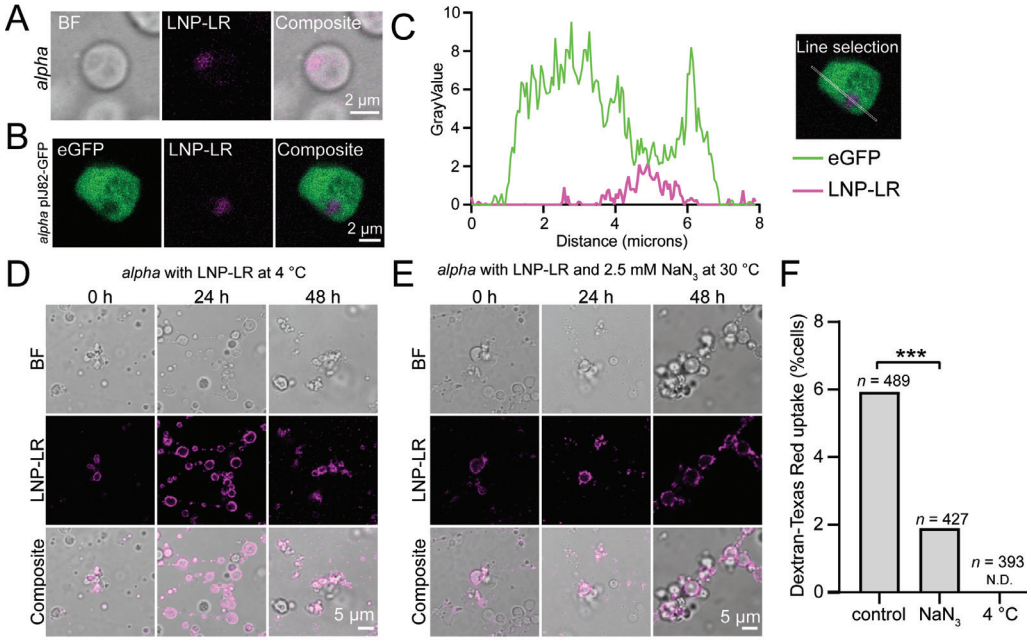

Figure 2. Localization of lipid nanoparticles in internal L-form vesicles

(A – B) Representative micrographs of localization of LNP-LR (Lipid nanoparticles containing 18:1 Liss Rhod PE; magenta) in internal vesicles of *alpha* (**A**; $n = 5$ observations) and *alpha* pIJ82-GFP (**B**; $n = 2$ observations) after an overnight and 72 h incubation experiment at 30 °C, respectively. See also Supplementary Fig. 2A – C. **(C)** Density profile plot of gray values (pixel intensity) of corresponding line selection of *alpha* pIJ82-GFP **(B)** incubated with LNP-LR showing that a decrease in cytoplasmic eGFP emission correlates with an increase in LNP-LR emission. **(D – E)** Localization of LNP-LR during incubation with *alpha* at 4 °C **(D)** or in the presence of 2.5 mM sodium azide (NaN_3) at 30 °C **(E)** after 0 h, 24 h and 48 h incubation. See Supplementary Fig. 2 D, E for control images. Similar results were obtained with 1 mM and 10 mM sodium azide (See Supplementary Fig. 3). Images were obtained from one experiment. **(F)** Percentage of *alpha* pIJ82-GFP cells showing Dextran-Texas Red (D-TR) uptake after 72 h incubation at 30 °C (control), in the presence of 2.5 mM sodium azide (NaN_3) or incubated at 4 °C. A significant reduction in D-TR uptake was observed for sodium azide (two-proportion z-test, $z = 3.111$, one-sided, $P = 0.00093$) and after incubation at 4 °C no uptake was detected (N.D.). Asterisks (***) indicate $P \leq 0.001$. The percentage of cells with D-TR uptake and total number of cells analysed is given for each condition and is based on combined cell counts from two replicate incubations. Note that incubation of L-forms with lipid nanoparticles (average size of 150 nm) results in their localization inside internal vesicles, and that uptake of external particles is inhibited by incubation at 4 °C or with sodium azide.

vesicles as detected by FIB-SEM (Fig. 3C, D, white arrow), in line with previous results (Fig. 1B). In addition, the composition of the cytoplasm and internal vesicle content was different, as measured using the InLens energy selective backscattered (EsB) detector which provides contrast based on the distribution of heavier elements (Fig. 3E). Analysis of the pixel intensity indicated that the contrast level inside the internal vesicle was similar to the extracellular environment, whereas the cytoplasm had a higher contrast. Moreover, an over-exposure experiment showed that the vesicle has the same capacity to absorb the electron dose as the medium outside, different from the rest of the cell (Supplementary Fig. 5A, B). These results

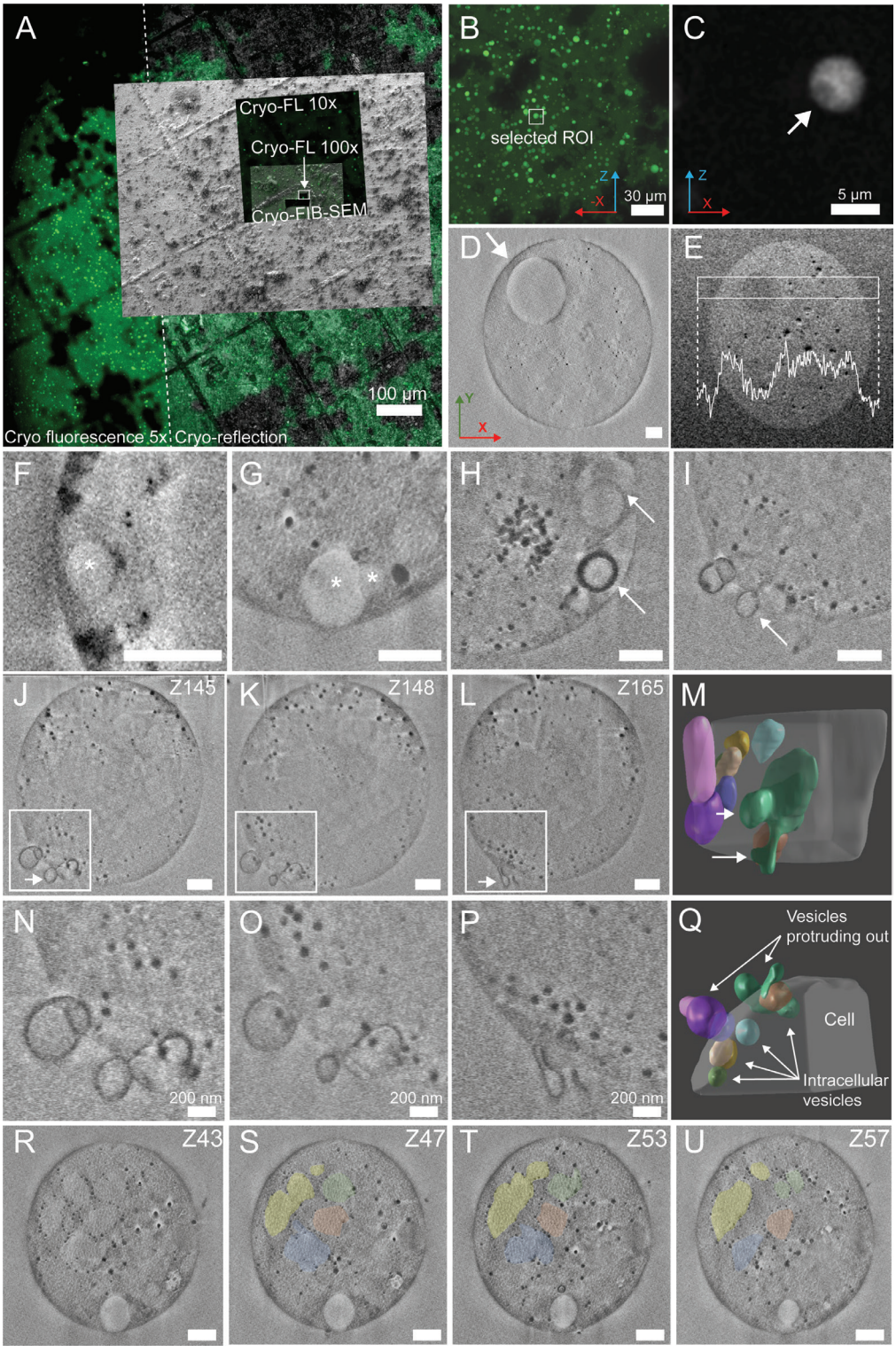
A
Cryo-FL 10x
Cryo-FL 100x
Cryo-FIB-SEM
100 µm
Cryo fluorescence 5x
Cryo-reflection
B
selected ROI
Z
X
30 µm
C
Z
X
5 µm
D
Y
X
E
F
G
H
I
J
Z145
K
Z148
L
Z165
M
N
200 nm
O
200 nm
P
200 nm
Q
Vesicles protruding out
Cell
Intracellular vesicles
R
Z43
S
Z47
T
Z53
U
Z57

◀ Figure 3. 3D cryo-fluorescence and cryo-FIB-SEM of L-forms reveals their ultra-structure in high resolution

(A) Example of correlated fluorescence and electron micrographs of *alpha* pIJ82-GFP (Zen Connect image) as performed with all imaged cells. A finderTOP raster visible both in fluorescence and electron microscopy facilitates alignment between the two imaging modules. Squares indicate different regions of interest, imaged at higher resolution. FIB-SEM: Focused Ion Beam - Scanning Electron Microscopy. FL: fluorescence light. **(B)** Example of higher resolution image of a selected region of interest (ROI), showing many fluorescent cells. **(C)** Fluorescence micrograph of the L-form depicted by white box in **(B)**, showing intracellular dark sphere (~1 µm, white arrow), as was performed to select all cells of interest. The X, Y and Z arrows in **(B – D)** indicate the 3D orientation of the imaged cell as observed in 3D FIB-SEM. **(D)** Scanning Electron Microscopy (SEM) image (SE, Inlens) of cell in **(C)** (size ~6 µm) with arrow indicating the internal vesicle (n = 1 cell). **(E)** Superposition of five consecutive slices (backscattered images) of cell in **(D)**. Inset: Density profile plot (white) of the average gray values (pixel intensity) for the region in the white box (n = 1 cell). **(F – I)** FIB-SEM slices showing different types of internal vesicles from three imaged cells. Vesicles lining the cell membrane of cells of around 3.5 µm in size **(F – G)**. Asterisks indicate vesicles in **(F, G)**. Vesicle complex **(H)** with different membrane thickness of vesicles indicated with white arrows. See also Supplementary Fig. 6A and Supplementary Movie 3. **(I)** Membrane protrusions as indicated with white arrow. **(J – Q)** Analysis of the interconnected vesicles of the cell in (I) (n = 1). **(J – L)** Three consecutive slices showing the interaction of different vesicles. (**N – P**) show higher magnification of the regions in white boxes in **(J – L)**, respectively. **(M, Q)** 3D segmentation of **(N – P)**. While some of the vesicles are intracellular, others protrude out of the cell. A complete connected vesicle structure is shown in green **(M, Q)** and indicated by white arrows **(I, J, L, M)**. See Supplementary Fig. 6B – D and Supplementary Movie 4. The cell in panels **H – Q** is around 4 µm in size. **(R – U)** Regions with different contrast (indicated by coloured regions) are lined with black particles representing putative lipid bodies as shown for one cell (similar regions observed in three cells). This cell is ~3.6 µm in size and relates to panel **(G)**. The size distribution of the black particles is 25 to 60 nm. Scale bars represent 500 nm unless otherwise specified.

support the finding that internal vesicles contain extracellular medium and are formed via membrane invagination (Fig. 1).

Further high-resolution imaging indicated the presence of multiple internal vesicles within individual cells (Fig. 3F – I, Supplementary Fig. 5C – E). Most detected vesicles were lining the cell membrane (Fig. 3G and Supplementary Fig. 5C – E), varied in size and membrane thickness (Fig. 3H) and could even be present inside larger vesicles (Fig. 3H and Supplementary Fig. 6A). The presence of vesicles within other vesicles has also been observed using fluorescence microscopy (Supplementary Fig. 1C, white arrow), showing a non-fluorescent vesicle within a larger vesicle encapsulating D-TR. In addition, vesicles could be observed budding out of the cell membrane (Fig. 3I). 3D reconstruction of the budding vesicles based on contour tracing revealed that they were either an extension of an internal vesicle, or remained connected to internal vesicles, forming a complex (Fig. 3J – Q, Supplementary Fig. 6A – D, and Supplementary Movies 3, 4).

In some cases, cells contained intracellular regions with different gray values from the rest of the cell (Fig. 3R – U). These regions had a size distribution of 300 to 800 nm, did not line the cell membrane, and were surrounded by dark particles of around 25 – 60 nm in diameter. It could be possible that the dark particles are lipid bodies, compared to previous cryo-FIB-SEM observations [308, 309]. A potential interpretation is that the internal regions are

vesicles of which the enclosing lipid membrane has partially degraded. The lipids and lipidic degradation products may have accumulated in lipid droplets that result in the observed black particles. To capture internal vesicle degradation, overnight timelapse imaging was performed on L-forms expressing cytoplasmic mCherry (*alpha* pRed*). Vesicles were identified by lack of cytoplasmic mCherry, and cells were imaged at different Z-heights to confirm that the vesicle had not simply moved location. Vesicle disruption was observed using 48 h L-forms resuspended in fresh LPB medium (Supplementary Fig. 7A, Supplementary Movie 5). Two more events of vesicle disruption were captured after performing a successive timelapse on the same sample, but with different cells (Supplementary Fig. 7B, C and Supplementary Movies 6, 7). All imaged vesicles were already present in the cells at the start of the timelapse. Whereas the time elapsed until vesicle disruption varied greatly (after 1 h or after 13 h and 17 h for the second experiment), the disruption process itself occurred within 15 min, which was the time interval between consecutive images. These findings strengthen the model that internal vesicles of L-forms can disrupt and, in this way, release their contents in the cytoplasm.

The internal vesicles observed in *K. viridifaciens* L-forms contain external medium and can be formed by the invagination of the cell membrane. L-forms can contain multiple vesicles of varying sizes, in some cases forming clusters or complexes of vesicles that can protrude out of the cell membrane. Internal vesicles may release their contents into the cell after vesicle degradation. These findings support a model for the uptake of macromolecules such as DNA by engulfment, followed by the release of the cargo after vesicle disruption (Fig. 4).

Discussion

The bacterial cell wall is an important protective barrier to the environment, providing stress resistance and enabling the selective passage of molecules. However, in recent years it has become clear that under some conditions, bacteria may also thrive without this layer. Prolonged exposure to environmental stresses, such as cell wall-targeting agents or a high osmotic pressure, can induce the formation of L-forms that efficiently proliferate without their cell wall [15, 95]. This drastic morphological shift enables some species of L-forms to take up DNA from their environment without relying on proteins homologous to canonical natural transformation machinery (Chapter 3). Here we provide evidence that L-forms may take up DNA and other macromolecules via engulfment and the subsequent formation of internal vesicles (Fig. 4), which is strongly reminiscent of endocytosis in eukaryotes.

Endocytosis is a fundamental and highly regulated process in eukaryotes that is involved in the uptake of nutrients, regulation of plasma membrane composition, sensing of the extracellular environment and signaling [261]. Invagination of the membrane followed by membrane scission and vesicle formation allows cells to internalize a wide array of cargo such

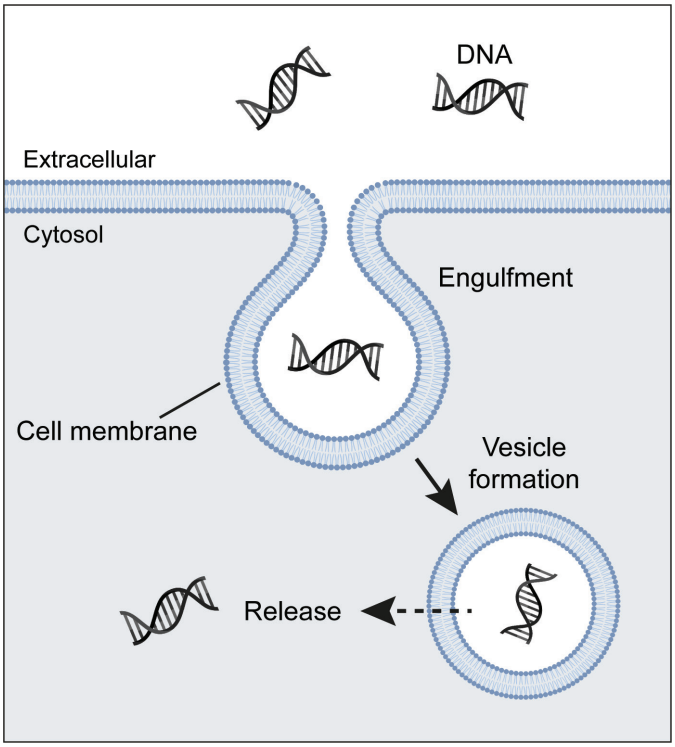

Figure 4. Proposed model for DNA uptake by internal vesicle formation in L-forms
Invagination of the cell membrane leads to the to the formation of internal vesicles in L-forms. As the cell membrane bulges inward, extracellular liquid, containing DNA or other macromolecules, is engulfed. The mechanism underlying the invagination process is energy-dependent and could be based on increased membrane synthesis and high membrane fluidity or mediated by proteins similar to those involved in eukaryotic endocytosis, such as cytoskeletal proteins. DNA is released from internal vesicles by an unknown process (indicated by dashed arrow), which may involve vesicle disruption. Image created with BioRender.com.

as fluids, ligands, plasma membrane proteins, and sometimes even entire bacteria. Invagination is often followed by passing the cargo through the endosomal pathway and lysosomal degradation [289]. Our work shows that L-forms use an endocytosis-like mechanism for the uptake of DNA, whereby membrane invagination leads to the formation of intracellular vesicles that, during their formation, encapsulated extracellular material (Fig. 4). Via this process, not only DNA but also other macromolecules such as 3 kDa dextran and even 150-nm lipid nanoparticles were encapsulated, strongly suggesting that the uptake process is non-specific. The uptake process is inhibited under conditions that reduce metabolic activity and energy production.

The exact mechanism underlying the formation of intracellular vesicles in L-forms is unknown but may depend on increased membrane dynamics due to excess membrane synthesis [89, 103]. An imbalance in the cell surface-to-volume ratio due to excess membrane

synthesis can lead to internal vesicle formation in spherical *Escherichia coli* and *B. subtilis* shape mutants [103, 310]. Internal vesicles or vacuoles can also be formed in enlarged protoplasts and spheroplasts (the latter containing an outer membrane) which are maintained under conditions that allow cell membrane expansion [311, 312]. Indeed, a lack of excess membrane production may also explain why we did not observe consistent DNA or dextran uptake in protoplasts and S-cells, both of which are unable to proliferate without their wall. However, we cannot exclude whether proteins similar to those involved in eukaryotic endocytosis, such as coat proteins, scission machinery, or cytoskeletal proteins [261], are involved in the formation of internal vesicles in L-forms. However, it must be noted that *B. subtilis* L-forms do not rely on known cytoskeletal proteins for membrane deformation and proliferation [102].

High-resolution electron microscopy revealed multiple internal vesicles inside L-form cells. Interestingly, the L-forms also contained regions not surrounded by a membrane but were lined with darker spots. These dark spots, which are generated by the local charging of the electrons with the material, were previously described as proteinaceous or lipid bodies [308, 309], and may originate from the degradation of the membrane of internal vesicles. The likely disintegration of internal vesicles was also captured using timelapse imaging. This disintegration would lead to release of the vesicle cargo into the cytoplasm. In eukaryotes, escape of therapeutics from endosomal vesicles can be mediated by bacterial, viral, and chemical agents or by nanoparticles [313, 314]. Escape mechanisms include pore formation, destabilization of the membrane, nanoparticle swelling, or osmotic rupture. High sucrose levels or the proton sponge effect facilitate the influx of protons followed by chloride ion accumulation and inflow of water, leading to rupture of the vesicle [315, 316]. Acidification of endosomes occurs via membrane-localized vacuolar ATPases (V-ATPases) that pump protons into the vesicles [317]. Bacteria have similar proton pumps called F-ATPases on their plasma membrane and have been found on the membrane of intracellular vesicles of enlarged protoplasts [318]. Considering the complexity of known escape mechanisms, further research is required to understand how internal L-form vesicles can disintegrate to release their contents into the cytoplasm.

Modern life forms are complex biological systems, which likely evolved from much simpler cells. Two model systems to study putative early life forms are giant lipid vesicles and L-forms due to their lack of a cell wall and biophysical way of proliferation [93, 94]. Horizontal gene transfer is thought to have played a pivotal role in the evolution of early life [319]. This may have occurred in cells that did not yet evolve a cell wall, allowing genetic recombination after cell fusion or lightning-triggered electroporation [320, 321], yet other mechanisms of HGT were unknown. Internal vesicles have been observed in L-forms of other bacterial species, with varying functions and mechanisms of vesicle formation described [262, 322]. L-forms of *Listeria monocytogenes* are capable of forming DNA-containing internal vesicles along the inside of the cell membrane, which upon release become metabolically active [17, 323]. Secondary

invagination of the vesicle membrane itself can result in vesicles containing cytoplasm and represent viable offspring. Similar to L-forms of *K. viridifaciens*, L-forms of *L. monocytogenes* produce internal vesicles via membrane invagination, which likely contain extracellular medium [89]. This bacterial species is not known to be naturally transformable, and does not contain a functional competence system [258]. This suggests that a similar endocytosis-like mechanism as observed for *K. viridifaciens* L-forms could be responsible for DNA uptake. These examples provide additional support for the existence of bacterial endocytosis.

A recent study reports similarities between spherical microfossils and wall-less cells [324]. When protoplasts were grown under conditions that mimic the presumed conditions of the Archean Eon, the period when life formed on Earth, intracellular vesicles were formed. Vesicle-like structures were also observed in 3.5 – 2.4 billion-year-old microfossils, suggesting that wall-less cells may have been present in ancient times. However, it should be noted that wall-less cells can also be formed from walled bacteria. For example, wall-less *Mycoplasma* have been shown to be derived from walled bacteria via degenerative evolution [325], and L-forms generated in the lab also originate from walled cells. L-forms may not have been the primordial cells themselves, but rather function as a model to study putative early life forms. Therefore, we propose that the endocytosis-like process observed in L-forms reflects an ancient mechanism of how primordial cells may have acquired new genetic material and nutrients via engulfment before the invention of the cell wall.

In conclusion, our work shows that the permanent loss of the bacterial cell wall allows the uptake of DNA, dextran, and 150-nm-sized lipid nanoparticles via internal vesicle formation. The invagination of the cell membrane leads to the engulfment of external material and subsequent vesicle formation. Eventually, the vesicle may disrupt, resulting in the release of the cargo into the cytoplasm. This is an energy-dependent process that has similarities to a simple form of endocytosis as seen in eukaryotes. Future studies are required to further elucidate the molecular mechanisms behind this process.

Materials and methods

Bacterial strains and culture conditions

All bacterial strains and plasmids used in this work are listed in Supplementary Table 3 and 4, respectively. L-forms were grown on solid L-phase medium agar (LPMA) or liquid LPB medium [15]. Liquid cultures for L-form growth in LPB medium were inoculated with a frozen aliquot of a 24 – 48 h L-form culture, and were grown for 72 – 96 h for chemical transformation and 168 h for all other experiments unless stated specifically. L-forms were adjusted to 5 – 7.5×10^7 CFU ml^{-1} for transformation assays (based on OD_{600} of 3 for 72 h and 168 h cells and 0.2 for 24 h cells), and 2.5 – 5×10^7 CFU ml^{-1} (OD_{600} of 2) for all other experiments

using 168 h cells. To obtain spores from *Kitasatospora viridifaciens* DSM40239 [221], the strain was grown confluently on maltose-yeast-extract medium (MYM) [222] for 72 – 96 h. S-cell formation was induced by growth of *K. viridifaciens* in liquid LPB medium inoculated at a density of 1×10^6 spores ml^{-1} at 100 rpm for 48 h [15]. All *Kitasatospora* strains were cultivated at 30 °C. Antibiotics were added to the culture medium to a final concentration of 100 μg ml^{-1} ampicillin, 50 μg ml^{-1} kanamycin, 25 μg ml^{-1} chloramphenicol, 5 μg ml^{-1} thiostrepton, 50 μg ml^{-1} apramycin, or 100 μg ml^{-1} hygromycin B (200 μg ml^{-1} hygromycin B for LB medium) when applicable. *E. coli* was grown in liquid cultures at 250 rpm or on solid LB medium at 37 °C. *E. coli* ET12567/pUZ8002 [273] was used to obtain methylation-deficient DNA for conjugation to *K. viridifaciens* and to extract DNA for transformation assays.

Construction of bacterial strains

K. viridifaciens pRed* was generated by intergeneric conjugation between *K. viridifaciens* DSM40239 and *E. coli* ET12567/pUZ8002 carrying the intergrative pRed* plasmid [278] as described in Kieser *et al*., (2000) [223]. In brief, *E. coli* was grown in LB medium containing kanamycin, chloramphenicol and apramycin to an OD_{600} between 0.4 – 0.6 at 37 °C, followed by resuspension in fresh LB medium. Around 10^8 spores of *K. viridifaciens* were resuspended in 500 μl 2 × YT broth (consisting of 10 g Bacto yeast extract, 16 g Bacto tryptone and 5 g NaCl per L). A heat shock was performed for 5 min at 42 °C before mixing the spores 1:1 with *E. coli* cells. After a brief centrifugation step, and removal of most of the supernatant, the cells were diluted in MilliQ and plated on mannitol soya flour medium (MS)(containing 20 g soya flour, 20 g mannitol and 20 g agar per L) [326] containing 10 mM $MgCl_2$. After incubation for 16 – 20 h, a selective overlay was performed with P-buffer [223], containing nalidixic acid to a final concentration of 20 μg ml^{-1} and apramycin to select for pRed*. After incubation, single colonies were grown on MYM medium containing apramycin, and acquisition of pRed* by *K. viridifaciens* was confirmed by fluorescent microscopy of liquid cultures.

L-form strains *alpha* and *alpha*Δ*divIVA* [86] were chemically transformed using PEG as described in Kieser *et al*., (2000) [223] using plasmid pIJ82-GFP (Chapter 3) to generate *alpha* pIJ82-GFP and *alpha*Δ*divIVA* pIJ82-GFP, respectively. The same method was utilized to generate *alpha* pRed*. Successful transformation was confirmed by growth on selective LPMA medium and fluorescence microscopy.

Preparation of protoplasts

To induce mycelial growth in liquid cultures for protoplast preparation, *K. viridifaciens* DSM40239 was inoculated at a density of 5×10^6 spores ml^{-1} in TSBS:YEME (1:1) medium supplemented with 0.5% (w/v) glycine [223] (Duchefa Biochemie) and 5 mM $MgCl_2$ (Duchefa Biochemie). TSBS contains 30 g L^{-1} Tryptone Soy Broth powder and 10% (w/v) sucrose while YEME (Yeast extract-malt extract medium) medium contains 3 g Difco yeast extract, 5 g Difco

Bacto-peptone, 3 g Oxoid malt extract, 10 g glucose, 340 g sucrose per Litre supplemented with 5 mM $MgCl_2 \times 6H_2O$ and 0.5% (w/v) glycine. After growth at 200 rpm for 48 h, the cells were washed with 10.3% (w/v) sucrose [223]. Protoplast formation was induced by addition of chicken egg-white lysozyme (~ 70,000 U mg^{-1}, Sigma-Aldrich) to a final concentration of 10 mg ml^{-1} and incubation for 2 – 3 h at 100 rpm and 30 °C. The cells were filtered through a sterile cotton wool filter to separate protoplasts from mycelial fragments. Where required, the protoplasts were concentrated by centrifugation at 1000×*g*. Protoplasts were always freshly prepared and used directly.

Isolation of S-cells

S-cell isolation was performed as described in Ramijan *et al*., (2018) [15]. Strains of *K. viridifaciens* were grown in LPB medium for 48 h to induce S-cell formation, followed by passing the culture through a sterile EcoCloth™ filter (Contec) to remove large mycelial aggregates and other debris if present. Subsequently, the culture was passed through a 5 µm Isopore™ membrane filter (Merck) to select for wall-less cells, followed by concentrating the cell suspension at 1000×*g* for 20 min. Around 90% of the supernatant was removed and the S-cells were resuspended in the remaining liquid. S-cells were always freshly prepared and used directly for experiments.

Transformation assay

Spontaneous DNA uptake in L-form strains *alpha* and *alpha*Δ*divIVA* was performed as described in Chapter 3. In brief, L-forms were incubated with 30 ng μl^{-1} unmethylated DNA (pFL-*ssgB*) or MilliQ for 24 h at 100 rpm and 30 °C. After incubation, cells were carefully resuspended, diluted in LPB medium and plated on selective and nonselective LPMA medium. Colony forming units were determined after incubation for 168 h. Transformation was verified by growth of a random selection of colonies on selective medium, as well as with PCR using primers Tsr_Hyg_FW1 and Tsr_Hyg_RV1. Cells were prepared from five individual replica cultures per strain to compare transformation efficiencies.

Preparation of fluorescently labelled DNA

Fluorescently labelled plasmid DNA was prepared using The Mirus Label IT® Cy™5 Labelling Kit (MIR 2725) according to the manufacturer's specifications. Aliquots of labelled DNA (100 ng μl^{-1}) were stored at −20 °C until further use.

Self-assembly of lipid nanoparticles

All lipids (DLin-MC3-DMA (Jayaraman 2012; Cholesterol, C8667, Sigma-Aldrich; Avanti Polar Lipids: DSPC, 850365, DMG-PEG2000, 880151, 18:1 Liss Rhod PE, 810150) were combined in a molar ratio of 50/38.3/10/1.5/0.2 using stock solutions (100 µM – 10 mM)

in chloroform:methanol (1:1 mix of chloroform, 22706, VWR Chemicals, and methanol, 83638, VWR Chemicals). Organic solvents were evaporated under a nitrogen stream and the remaining solvent was removed *in vacuo* for at least 1 h. Subsequently, the lipid film was dissolved in $EtOH_{abs}$ (20821, VWR Chemicals) and a 50 mM citrate buffer (pH = 4, MilliQ; using citric acid, C0759, and sodium citrate tribasic dehydrate, C7254; Sigma-Aldrich) was prepared. Each solution was loaded into separate syringes and connected to a T-junction microfluidic mixer. The solutions were mixed in a 3:1 flow ratio of citrate buffer against lipids (1.5 mL min^{-1} for citrate buffer, 0.5 mL min^{-1} for lipid solutions) giving a total lipid concentration of 1 mM. After mixing, the solution was directly loaded in a 10k MWCO dialysis cassette (Slide-A-Lyzer™, Thermo Scientific) and dialyzed overnight against 1× Phosphate Buffered Saline (PBS), containing 137 mM NaCl (NAC02, Formedium), 2.7 mM KCl (1.04936, VWR Chemicals), 8 mM Na_2HPO_4 (1.06586, VWR Chemicals), and 2 mM KH_2PO_4 (60229, Sigma-Aldrich), overnight. Lipid nanoparticles (LNP-LR) are available from the corresponding authors on reasonable request. All incubations with LNPs were performed with cells resuspended in LPB medium of which the final volume of LNP solution was 25%.

Hydrodynamic diameter and zeta-potential measurements

Preparations of lipid nanoparticles were characterized in the following manner (Supplementary Table 5). Dynamic light scattering (DLS) measurements were performed on a Zetasizer Nano Series S (Malvern Instruments, Malvern, UK). The incorporated HeNe laser works at a wavelength of 633 nm and uses a detector at an angle of 173° (noninvasive backscatter technology). Measurements were recorded with 1 min equilibration time in UV cuvettes at 25 °C. For the estimation of z-average diameter (intensity weight mean diameter) and polydispersity index (PDI) (relative width of particle size distribution), samples were prepared by tenfold dilution with 1× PBS. For the estimation of the zeta potential, the sample was diluted with 0.1× PBS and measured in a Zetasizer Nano Series SZ (Malvern Instruments, Malvern, UK). All the data were in triplicates to obtain the mean value.

Fluorescence and light microscopy

All microscopy was performed using a Zeiss LSM 900 confocal microscope with Airyscan 2 module, temperature control chamber, and Zeiss Zen 3.1 software (blue edition, Carl Zeiss Microscopy GmbH). The excitation and emission settings are listed in Supplementary Table 6. Multichannel (DIC and fluorescence) and multistack images were obtained unless specified otherwise. Around 10 µl of cells were imaged on a µ-Slide 8 Well Ibidi® slide coated with 0.1% (w/v) poly-L-lysine (Sigma-Aldrich). Excess poly-L-lysine was removed, and the slide was allowed to dry before sample application. For timelapse imaging or overnight incubation in the temperature control chamber, 400 µl of cell culture added to a 35 mm imaging µ-Dish (Ibidi®) and allowed to settle at 30 °C for 1 h before overnight imaging. Image analysis was

performed using Fiji (ImageJ) software [282].

Uptake of fluorescently labelled DNA was assessed by incubating cells with Cy5-labelled plasmid DNA (pFL-*ssgB*) at a final concentration of 1.25 μg ml^{-1} and was imaged in a μ-Dish (Ibidi®) after 72 h. Chromosomal DNA was visualized after incubation for 30 min with SYTO 9 (Invitrogen) at a final concentration of 2 μM. Cell membranes were visualized by incubation with SynapseRed C2M (SynapseRed, PromoKine, PromoCell GmbH) at a final concentration of 40 μg ml^{-1}. After overnight incubation in a μ-Dish (Ibidi®) using the Zeiss LSM 900 confocal temperature control chamber, cells were imaged using the Airyscan mode with super resolution post-image processing via the Zen software. Protoplasts and S-cells were incubated with SynapseRed up to 72 h before imaging on a glass slide.

Quantification of putative internal vesicles was performed after incubating 168 h L-forms (*alpha* pRed*) or freshly harvested S-cells and protoplasts (*K. viridifaciens* pRed*) producing cytoplasmic mCherry with SynapseRed for 0 or 72 h. SYTO 9 was added directly before imaging to identify DNA. Cells were placed on a μ-Slide 8 Well Ibidi® slide coated with 0.1% poly-L-lysine. L-forms and S-cells were imaged from top to bottom with a step size of 0.5 μm and protoplasts with a step size of 0.28 μm to account for their smaller cell size. Cells having one or more regions lacking mCherry, SYTO 9 or SynapseRed staining were counted as a cell with a putative internal vesicle using the Cell Counter plugin in Fiji (ImageJ).

To capture internal vesicle formation and uptake of Dextran-Texas Red (D-TR, D-3329, 3000 MW, neutral, Molecular Probes), cells of *alpha* pKR2 were incubated with a final concentration of 1 mg ml^{-1} D-TR in PBS and were imaged overnight. Multistack imaging across 6 μm total distance with 1.5 μm steps was done with an image captured every 10 min. Imaging of D-TR uptake in L-forms, protoplasts, or S-cells was performed after incubation up to 72 h. Quantification of the percentage of cells that had taken up D-TR was performed as following. Cells producing cytoplasmic eGFP were incubated with PBS or 1 mg ml^{-1} D-TR in duplo for 72 h (168 h *alpha* pIJ82-GFP or freshly harvested S-cells or protoplasts from *K. viridifaciens* pIJ82-GFP). Cells were diluted ten times in LPB medium and gently centrifuged for 10 min at 1000×*g*, after which the supernatant was replaced by LPB medium. Cells were placed on a μ-Slide 8 Well Ibidi® slide coated with 0.1% poly-L-lysine. Z-stack images were acquired from top to bottom of the cells with 0.28 μm steps. Cells with putative D-TR uptake were identified as those lacking a region of cytoplasmic eGFP (putative internal vesicle) while revealing an increased D-TR emission at this region as measured using the Plot Profile tool in Fiji (ImageJ). Cells with and without uptake were counted using the Cell Counter plugin in Fiji (ImageJ).

Uptake of red fluorescent LNPs (LNP-LR) by *alpha* was visualized by imaging after overnight incubation in a μ-Dish (Ibidi®) or after incubation for up to 72 h prior to imaging as indicated. Inhibition of LNP uptake was performed by incubation in the presence of 1 mM, 2.5 mM, or 10 mM sodium azide (Sigma-Aldrich) or incubation at 4 °C, and images

were obtained via the Zen software after 0 h, 24 h, and 48 h. To determine the subcellular localization of LNP-LR in *alpha* pIJ82-GFP, imaging was performed using the Airyscan mode with super-resolution post-image processing and analyzed using the pixel intensity of the red (LNP-LR) and green (eGFP) channels using the Plot Profile tool in Fiji (ImageJ).

To capture vesicle disruption, L-forms were resuspended in fresh LPB medium to an OD_{600} of 0.04. Dilutions were placed in a 96-wells black/glass bottom SensoPlate and gently spun down for 5 min at 1000×*g* to settle the cells at the bottom of the wells. Cells were imaged using a Lionheart FX automated microscope (BioTek) with Gen 5 v.3.10 software at a magnification of 60× air (brightfield and mCherry using Texas Red 586/647 filter cube). Z-stack images were captured every 15 min with a step size of 1 µm covering 12 µm total for 20 h (Supplementary Movie 5) or a step size of 0.5 µm covering 5 µm total for 17.5 h (Supplementary Movies 6, 7).

Cryo-correlative fluorescence and electron microscopy

High-pressure freezing

A 168 h culture of the L-form strain *alpha* pIJ82-GFP expressing cytoplasmic eGFP was adjusted to OD_{600} of 2 in fresh medium containing 25% (v/v) PBS and a final concentration of 17% (w/v) sucrose. Cells were incubated for 96 h, during which cells settled to the bottom. A few microliters of the resuspended L-form pellet were sandwiched between HPF (high-pressure-freezing) carriers with 2 mm internal diameter (either 0.1 mm or 0.05 mm cavity, Art. 241 and Art. 390 respectively, Wohlwend) and tailor-made grid labelled, flat-sided finderTOP (Alu-platelet labelled, 0.3 mm, Art.1644 Wohlwend) to allow an imprint of a finder matrix on the amorphous ice [327]. The finderTOP was treated with 1% L-α-phosphatidylcholine (61755, Sigma-Aldrich) in ethanol (1.00983.1000, Supelco) before freezing. The samples were then high-pressure frozen (Live µ, CryoCapCell) and stored in liquid nitrogen until imaging.

To improve the correlation between cryo-light and cryo-electron microscopy, the frozen samples were loaded into a universal cryo-holder (Art. 349559-8100-020, Zeiss cryo accessory kit) using the ZEISS Correlative Cryo Workflow solution, fit into the PrepDek® (PP3010Z, Quorum technologies, Laughton, UK). Here, the HPF carriers fits into a universal cryo-holder, which subsequently can be placed into an adapter specific for cryo-light or cryo-electron microscopy.

Cryo-fluorescence imaging to detect regions of interests (ROI)

The frozen samples were imaged with a cryo-stage adapter (CMS-196, Linkam scientific inc.) applied to an upright confocal microscope (LSM 900, Zeiss microscopy GmbH) equipped with an Airyscan 2 detector. Overview images (Zeiss C Epiplan-Apochromat 5×/0.2 DIC) were made with reflection microscopy to visualize the gridded pattern on the ice surface. Next, medium-resolution Z-stack images (Zeiss C Epiplan-Apochromat 10×/0.4 DIC) were

taken with a 488 nm laser (0.4%) with a voxel size of 0.15 µm × 0.15 µm × 1.18 µm. Using this resolution, cells of interest could be selected and Z-stack images were created (Zeiss C Epiplan-Neofluar 100×/0.75 DIC) using a 488 nm laser (4%), with a voxel size of 0.08 µm × 0.08 µm × 0.44 µm. In addition, the ice surface was imaged in all ROIs with reflection microscopy for correlation purposes in the FIB-SEM. Prior to cryo-light imaging, a Zeiss ZEN Connect project (Zeiss software for correlative microscopy, version 3.1) was created to make a working sheet (canvas) to align and overlay all the images and to facilitate further correlation with cryo-FIB-SEM.

3D Cryo-FIB-SEM

The sample was sputter-coated with platinum, 5mA current for 30 s, using the prep stage sputter coater (PP3010, Quorum technologies, Laughton, England) and was transferred into the Zeiss Crossbeam 550 FIB-SEM (Carl Zeiss Microscopy GmbH, Oberkochen, Germany) using the PP3010T preparation chamber (Quorum, Laughton, England). Throughout imaging, the samples were kept at −140 °C and the system vacuum pressure was 1×10^{-6} mbar.

After inserting the sample into the FIB-SEM chamber, overview images were taken using the SEM to align the data with the LSM reflection image of the surface of the same ZEN Connect project. This alignment enables the stage registration, which allows using the fluorescence signal to navigate to different regions of interest. After initial alignment using the SEM, a FIB image of the surface was collected with the 30kV@10 pA probe in 54° tilt.

A coarse trench was milled for SEM observation using the 30 kV@30 nA FIB probe. The cold deposition was done with platinum for 30 sec. Fine FIB milling on the cross-section was done using the 30kV@700 pA probe. For serial FIB milling and SEM imaging the slice (trench) width was 40 µm and for FIB milling the 30 kV@300 pA probe was used, with a slice thickness of 20 nm. When a new slice surface was exposed by FIB milling, an InLens secondary and EsB images were simultaneously collected at 2.33 kV acceleration potential with 250 pA probe current. The EsB grid was set to −928 V. The image size was set to 2048 × 1536 pixels. For noise reduction line average with a line average count $n = 46$ at scan speed 1 was used. The voxel size of all stacks was $5\ nm^3 \times 5\ nm^3 \times 20\ nm^3$.

3D FIB-SEM Image post processing

The cryo-FIB-SEM images were processed using MATLAB (R2018b, Natick, Massachusetts: The MathWorks Inc.) to correct for defects such as curtaining, misalignment, and local charging. The same software was used for subsequent noise reduction and contrast enhancement. A summary of each processing step is as following:

Curtaining: Removing the vertical stripes in the stacks was done following a wavelet-FFT filtering approach [328]. In brief, the high-frequency information corresponding to the

vertical stripes was successively condensed into a single coefficient map using decomposition by the coif wavelet family. Subsequently, a 2D-fourier transform was performed to further tighten the stripe information into narrow bands. Finally, the condensed stipe information was eliminated by multiplication with a gaussian damping function and the destriped image was reconstructed by inverse wavelet transform.

Alignment: The consecutive slices were aligned using normalized cross-correlation. Briefly, the first image in the stack was chosen as the reference and the second image was translated pixel by pixel across the reference and a normalized cross-correlation matrix was obtained using the normxcorr2 function. The location of the highest peak in the cross-correlation matrix (representing the best correlation) was then used to calculate the translation required to align the two images. Once the moving image was aligned with the reference image, it served as the reference for the alignment of the subsequent slice.

Charging: Elimination of the local charge imbalance was achieved using anisotropic gaussian background subtraction. Briefly, the imgaussfilt function was used to perform 2D-gaussian smoothing with a two-element standard deviation vector. The elements in the vector were chosen in a manner to apply a broad and sharp gaussian in the horizontal and vertical directions, respectively. Subsequently, the corrected image was obtained by subtracting the filtered image from the original image.

Noise Reduction: In order to improve the signal-to-noise ratio, noise reduction was performed using anisotropic diffusion filtering [329]. Briefly, using the imdiffuseest function, the optimal gradient threshold and the number of iterations required to filter each image was estimated. Subsequently, the imdiffusefilt function was applied with the estimated optimal parameter values to denoise each image.

Contrast enhancement: As the final processing step, the contrast was enhanced using Contrast-limited adaptive histogram equalization [330]. Using the adapthisteq function, the contrast was enhanced in two steps, using a uniform distribution and a low clipping limit in order to avoid over-amplification of homogeneous regions.

3D segmentation: DragonflyTM image analysis and deep-learning software (version 2021.1, Objects Research Systems, Montreal, QC, Canada) was used to segment all image data.

Statistics

All statistics were performed using the software SPSS statistics (IBM, version 27.0) with a significance level of 0.05. Data normality was tested using Shapiro-Wilk and Kolmogorov–Smirnov tests as well as Q-Q plots where applicable. Homogeneity of variances was tested using Levene's test. The means, and standard deviations were calculated via Graphpad Prism v. 9.0.0. or Excel (version 2016).

Supplementary Data

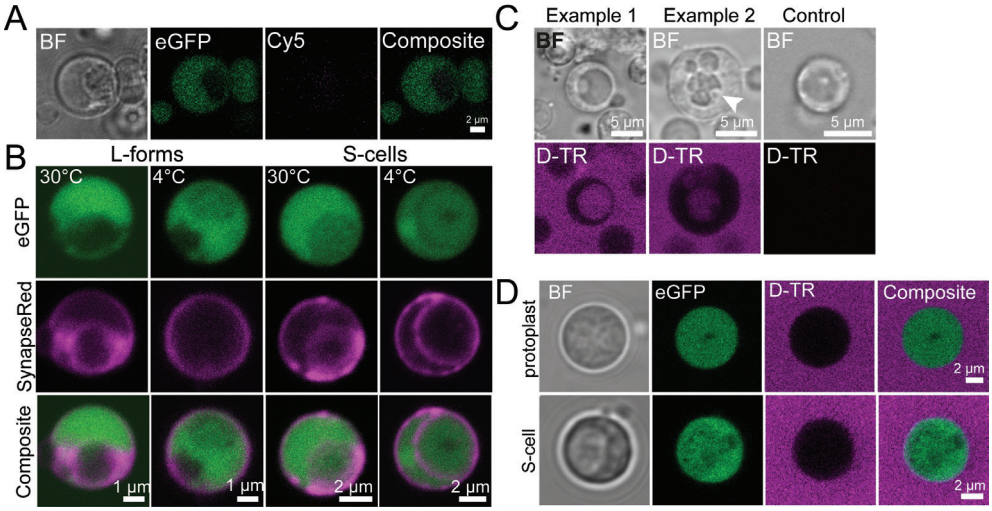

Supplementary Figure 1. Comparison of SynapseRed staining and dextran uptake in wall-deficient cells, and Cy5-DNA imaging control

(A) Representative micrograph of *alpha* pIJ82-GFP incubated for 72 h without Cy5 DNA (Cy5, magenta) as fluorescence control (25 cells imaged from one incubation). BF = brightfield. **(B)** Representative images of 168 h L-form *alpha* pIJ82-GFP and S-cells of *K. viridifaciens* pIJ82-GFP after 72 h incubation with SynapseRed at 30 °C or 4 °C (a minimum of five observations per condition from two independent experiments). SynapseRed stains internal membranes at both temperatures in S-cells but only at 30 °C in L-forms. **(C)** *alpha* incubated with (example 1 and 2) or without (control) Dextran-Texas Red (D-TR; magenta) for 64 h, showing the formation of internal vesicles filled with D-TR (eight observations from one incubation). The arrow indicates the presence of a non-fluorescent secondary internal vesicle inside an existing internal vesicle (example 2, one observation). **(D)** Protoplasts and S-cells of *K. viridifaciens* pIJ82-GFP incubated with D-TR for 72 h. Note that no internalization of D-TR was observed (at least 100 protoplasts and 10 S-cells from one experiment).

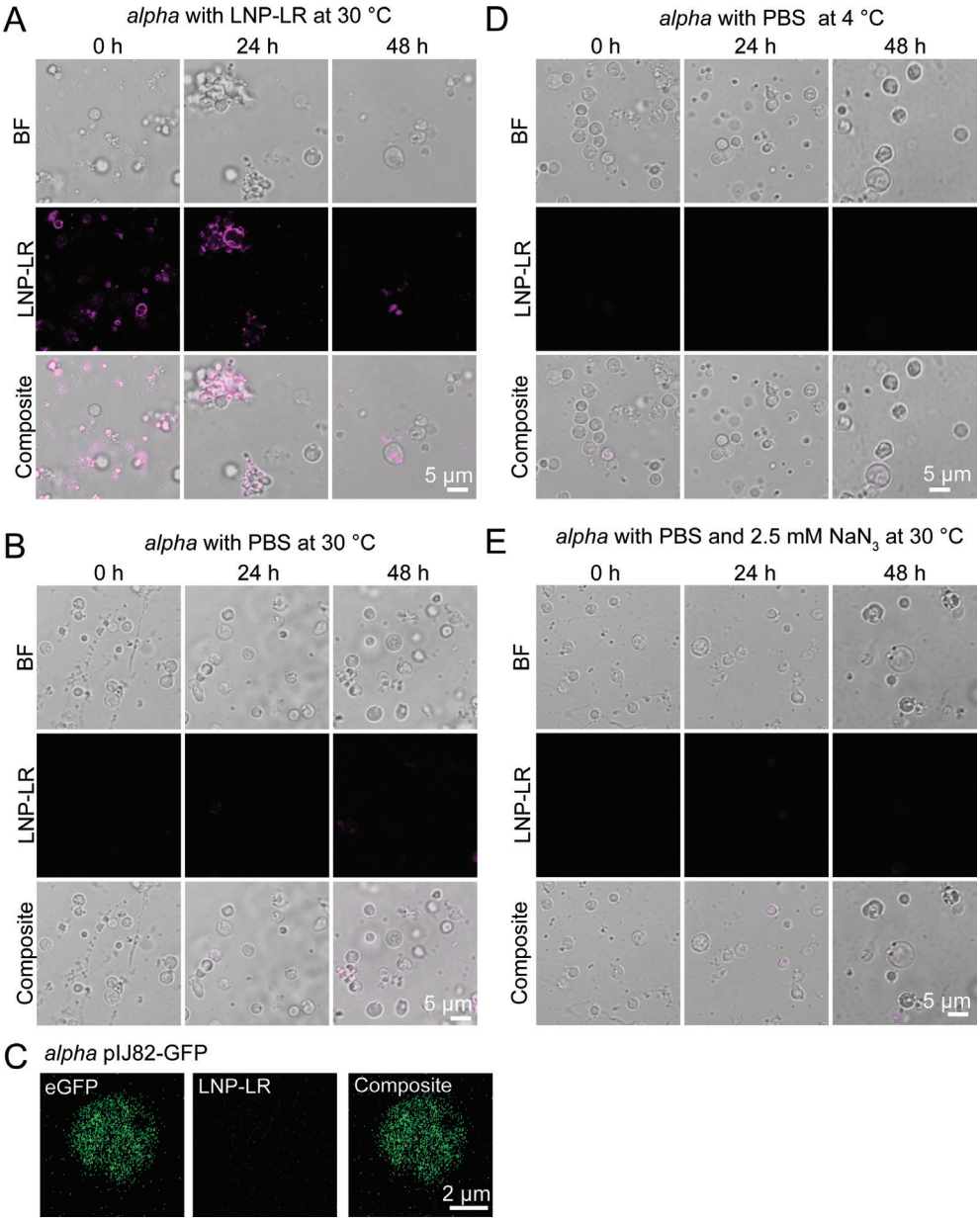

Supplementary Figure 2. Uptake of LNP-LR by *alpha*

(A – B) *alpha* incubated with LNP-LR (LNP-Liss Rhod; magenta) **(A)** or PBS (Phosphate Buffered Saline) **(B)** at 30 °C showing localization of LNP-LR after 0 h, 24 h and 48 h and examples of autofluorescence, respectively, related to Fig. 2A. Images were obtained from one experiment. **(C)** *alpha* pIJ82-GFP incubated for 72 h without LNP-LR as imaging control for Fig. 2B (one experiment with three control cells). **(D – E)** *alpha* incubated with PBS at 4 °C **(D)** or with PBS at 30 °C in the presence of 2.5 mM sodium azide (NaN_3) **(E)** as control for fluorescence emission of cells in Fig. 2D and E, respectively.

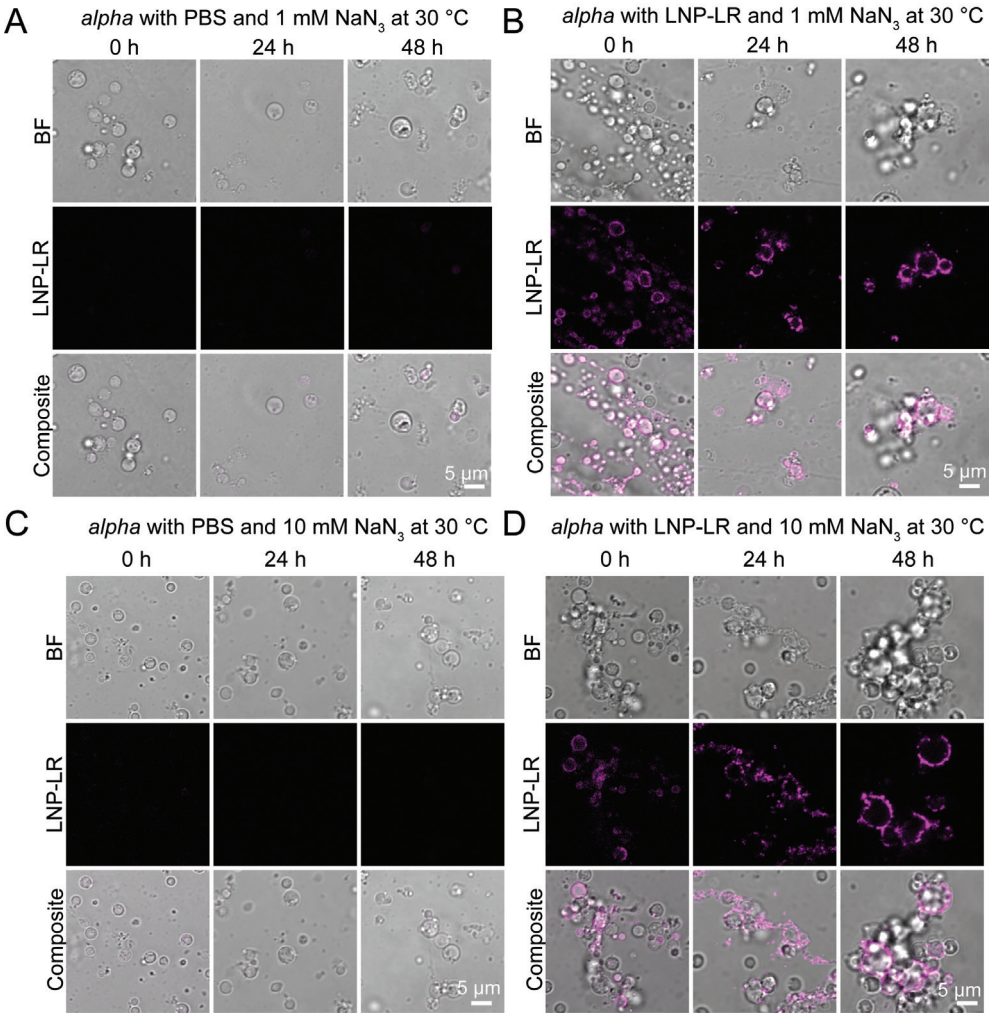

Supplementary Figure 3. Incubation of *alpha* with LNP-LR in the presence of sodium azide
(A – D) *alpha* incubated with PBS (Phosphate Buffered Saline) or LNP-LR (LNP-Liss Rhod; magenta) at 30 °C with 1 mM or 10 mM sodium azide as indicated. Images were obtained after 0 h, 24 h and 48 h incubation from one experiment.

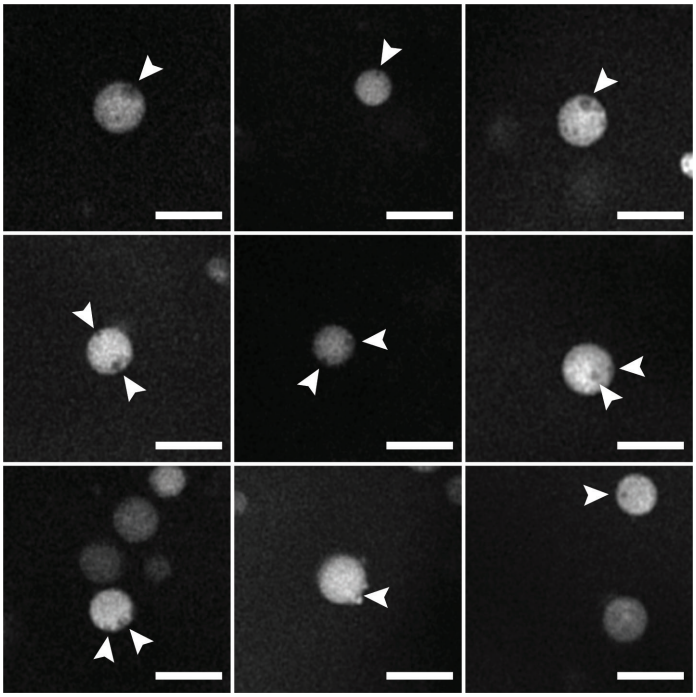

Supplementary Figure 4. High resolution cryo-fluorescence of L-forms

Examples of *alpha* pIJ82-GFP cells (n = 9) imaged using cryo-fluorescence microscopy (eGFP emission depicted in grey), originating from four regions of interest (from a total of six regions). Putative vesicles are indicated with arrows. Images were captured using the long distance 100× objective. Scale bars indicate 5 μm.

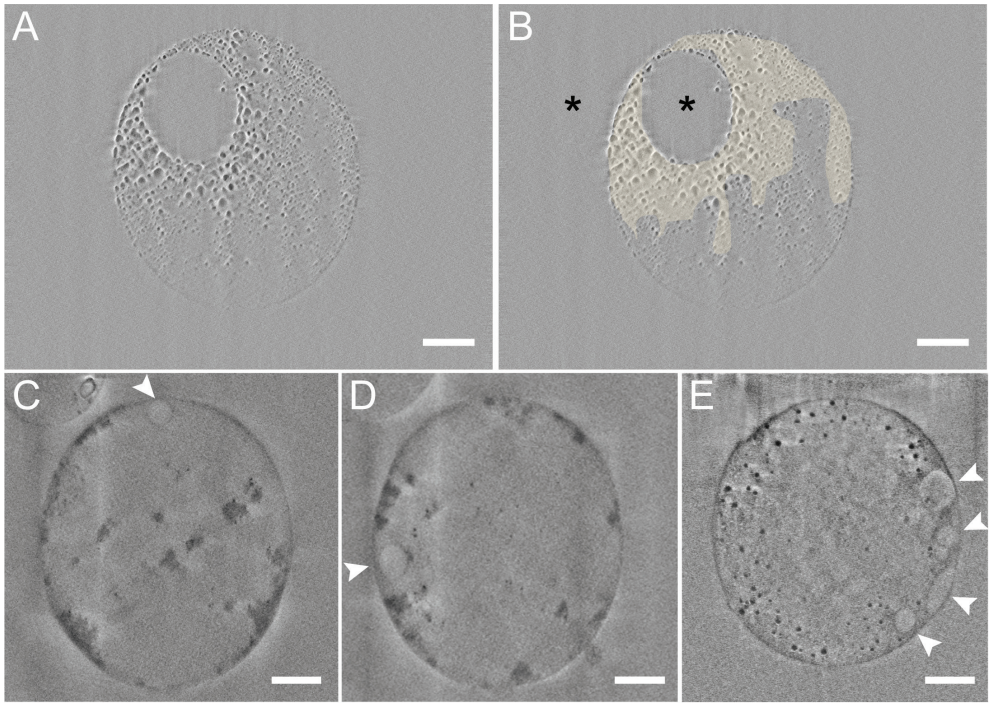

Supplementary Figure 5. Over-dose experiment of L-form cell using FIB-SEM and L-form vesicles
(A – B) FIB-SEM slice of over-dose experiment using *alpha* pIJ82-GFP (performed for one cell). The yellow colour in **(B)** indicates areas with distinguished beam damage. The vesicle (indicated by black asterisk inside the cell) seems to be less to none affected by the over-dose, similar to the medium outside the cell (black asterisk outside of the cell). The image in Fig. 3D was taken before this experiment, and Fig. 3E is obtained by summing several slices deeper in the cell after acquiring this image. Scale bar indicates 1 μm. **(C – E)** FIB-SEM slices of two cells in which **(C, D)** correspond to the cell in Fig. 3F and **(E)** corresponds to the cell in Fig. 3H – K. White arrows indicate vesicles that line the cell membrane (three slices of two imaged cells shown). Scale bar in **(C – E)** indicates 500 nm.

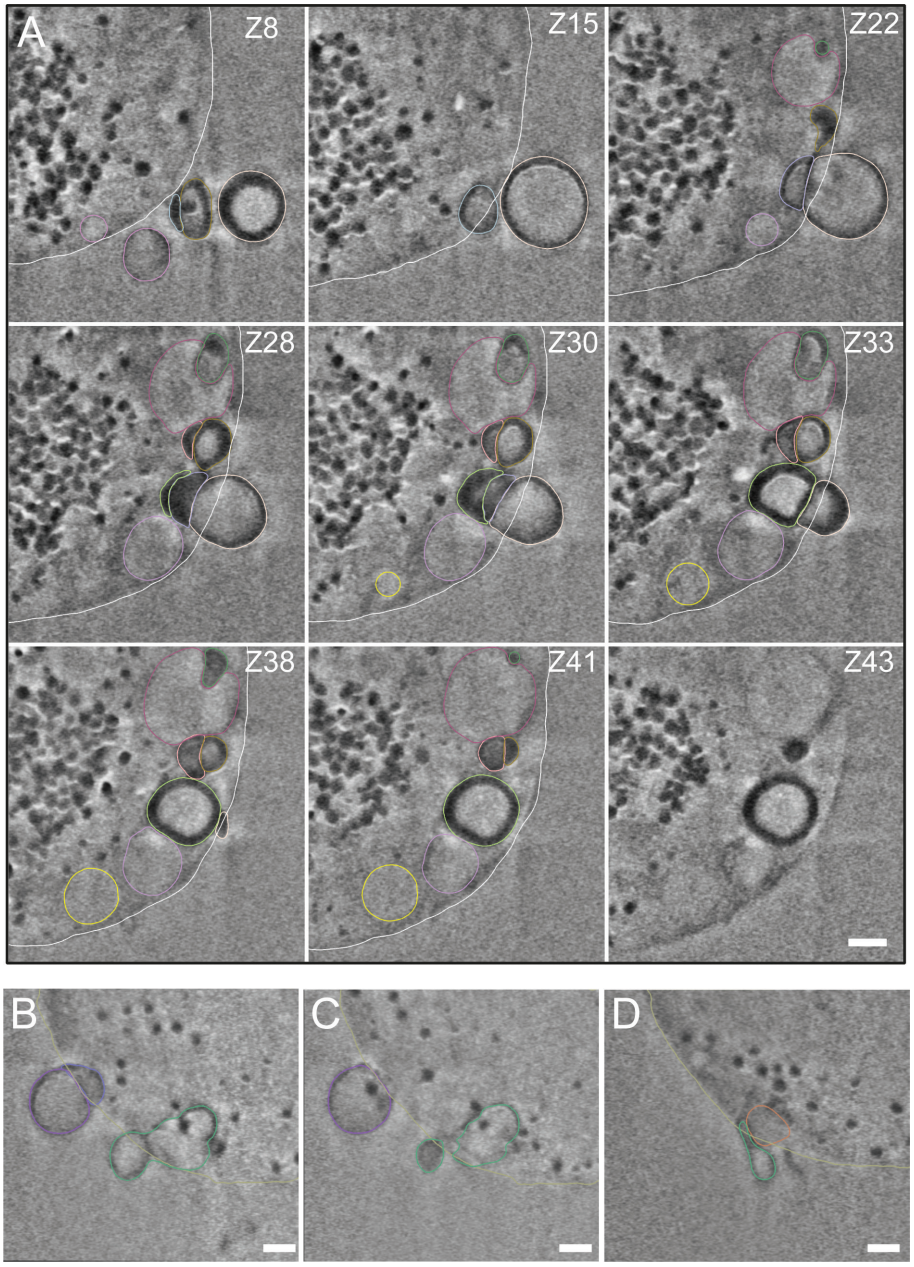

Supplementary Figure 6. 3D Segmentation of L-form vesicles

(A) FIB-SEM slices corresponding to the cell in Fig. 3H. Z-number indicates the slice. Colours indicate individual vesicles. See also Supplementary Movie 3. **(B – D)** FIB-SEM slices corresponding to Fig. 3I – Q, respectively. Colours correspond to the segmented colours in Fig. 3M, Q. Vesicles that are budding out the cells are connected to other vesicles or are elongated inside the cell. See also Supplementary Movie 4. 3D segmentation as shown in **(A – D)** was performed for two different regions of one cell. Scale bars indicate 200 nm.

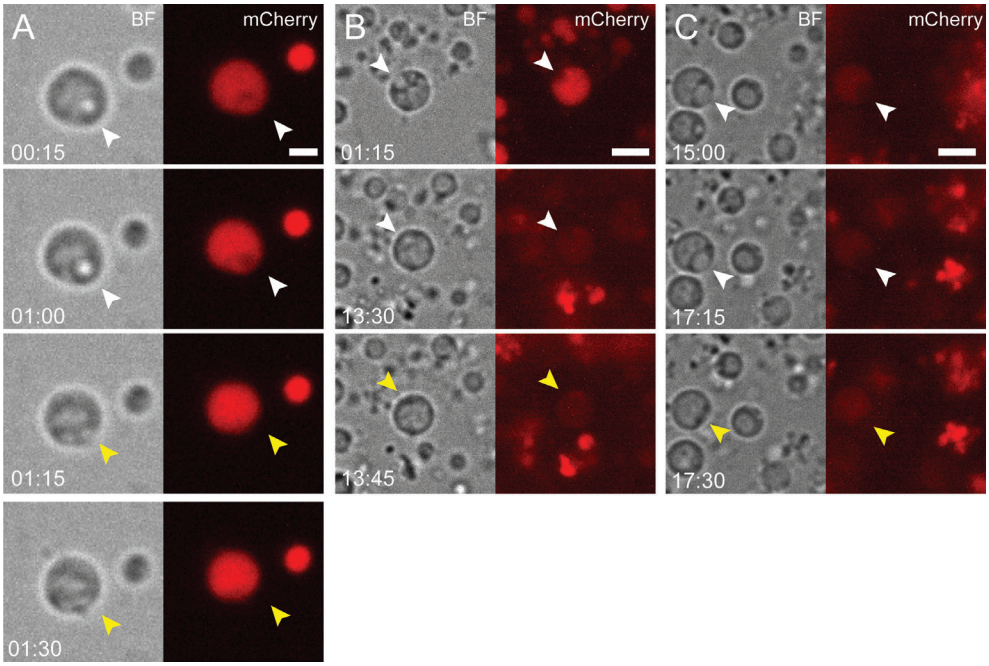

Supplementary Figure 7. Timelapse of putative vesicle disruption in L-form cells

(A – C) Stills from timelapse experiment of *alpha* pRed* expressing cytoplasmic mCherry. Elapsed time is indicated in h:min. Putative vesicle disruption is observed between 01:00 to 01:15 h:min **(A)**, 13:30 to 13:45 h:min **(B)** and 17:15-17:30 h:min **(C)**. White arrows indicate vesicles, yellow arrows indicate the lack of vesicles. All vesicles were present from the start of the incubation. Cells were incubated at 30 °C and imaged overnight using the Lionheart FX automated microscope. Images were taken every 15 min for 20 h **(A)** or 17.5 h **(B, C)**. Left: Brightfield. Right: mCherry emission. Scale bars indicate 2 µm **(A)** and 5 µm **(B, C)**. See also Supplementary Movie 5, 6 and 7.

Supplementary Table 1. Quantification of internal vesicles

Quantification of the percentage of 168 h L-form cells (*alpha* pRed*), freshly harvested S-cells and protoplasts (*K. viridifaciens* pRed*) with internal vesicles with SynapseRed, imaged directly after addition or after 72 h incubation and stained with SYTO 9. Integer numbers indicate the number of cells with or without internal vesicles. The percentage of cells with putative internal vesicles is given (positive %).

Cell type	No incubation				72 h incubation			
	Vesicle	No vesicle	Total	Positive (%)	Vesicle	No vesicle	Total	Positive (%)
L-forms	50	154	204	24.51	37	215	252	14.68
S-cells	5	218	223	2.24	9	337	346	2.60
Protoplasts	1	203	204	0.49	1	237	238	0.42

Supplementary Table 2. Quantification of Dextran-Texas Red uptake

Quantification of the percentage of cells that take up Dextran-Texas Red (D-TR) after a 72 h incubation (positive %). L-forms (168 h, *alpha* pIJ82-GFP), S-cells and protoplasts (*K. viridifaciens* pIJ82-GFP) were incubated in duplo (replica 1 and 2) with Phosphate Buffered Saline (PBS, control) or D-TR. The number of cells with or without uptake of D-TR are indicated.

Cell type	Condition	Replica	Uptake	No uptake	Total cells counted	Positive (%)
L-forms	PBS	1	0	101	101	0.0
		2	0	602	602	0.0
	D-TR	1	18	284	302	6.0
		2	11	176	187	5.9
S-cells	PBS	1	0	75	75	0.0
		2	2	94	96	2.1
	D-TR	1	5	295	300	1.7
		2	1	114	115	0.9
Protoplasts	PBS	1	0	168	168	0.0
		2	1	127	128	0.8
	D-TR	1	2	186	188	1.1
		2	0	79	79	0.0

Supplementary Table 3. Strains used in this study

Strain	Description	Notes/references
Escherichia coli ET12567/ pUZ8002	Methylation-deficient strain (F^-, *dam*-13::*Tn*9, *dcm*-6, *hsdM*, *hsdR*, *recF*143, *zjj*-202::Tn10, *galK*2, *galT*22, *ara*14, *lacY*1, *xyl*-5, *leuB*6, *thi*-1, *tonA*31, *rpsL*136, *hisG*4, *tsx*-78, *mtl*-1, *glnV*44) carrying the non-transmissible pUZ8002 plasmid	273
Kitasatospora viridifaciens DSM40239	Wild-type strain	DSMZ, 221
K. viridifaciens pIJ82-GFP	*K. viridifaciens* DSM40239 containing pIJ82-GFP	Chapter 3
K. viridifaciens pRed*	*K. viridifaciens* DSM40239 containing pRed*	This work
alpha	L-form derivative of DSM40239 obtained after exposure to Penicillin G and lysozyme	15
alpha pIJ82-GFP	*alpha* carrying pIJ82-GFP	This work
alpha pRed*	*alpha* carrying pRed*	This work
alpha pKR2	*alpha* carrying pKR2, which contains a C-terminal eGFP gene fusion to *divIVA* under the control of the *Streptomyces coelicolor gap1* promoter	86
*alpha*Δ*divIVA*	divIVA::aac(3)IV	86
*alpha*Δ*divIVA* pIJ82-GFP	*alpha*Δ*divIVA* containing pIJ82-GFP	This work

Supplementary Table 4. Plasmids used in this study

Plasmid	Features	Notes/References
pRed*	pIJ8630-derivative expressing *mCherry* under control of the *S. coelicolor A3(2) gap1* promoter	278
pIJ82-GFP	pSET152-derivative expressing *eGFP* under control of the *S. coelicolor gap1* promoter	Chapter 3
pFL-*ssgB*	pWHM3-oriT-hyg-derivative containing a hygromycin resistance gene and a downstream flanking sequence of *ssgB* downstream derived from pKR1 to enable integration into the genome	Chapter 3
pKR2	pIJ8630 derivative carrying a viomycin resistance cassette and expressing a C-terminal *eGFP* fusion to *divIVA* under control of the *S. coelicolor* A3(2) *gap1* promoter	86

Supplementary Table 5. Characterization of lipid nanoparticles
Dynamic Light Scattering (DLS) and ζ-potential of lipid nanoparticles. PDI = polydispersity index.

LNP	Avg. size (nm) at 25 °C	PDI	ζ-potential (mV) at 25 °C
LNP-LR	151.1	0.144	−8.52

Supplementary Table 6. Imaging settings used with the Zeiss LSM 900 confocal microscope

Fluorescent protein, dye or particle	Excitation (nm)	Emission filter (nm)
eGFP	488	490 – 575
mCherry	561	565 – 700
SYTO 9	488	490 – 575
SynapseRed C2M	488	571 – 700
Dextran-Texas Red	561	560 – 700
Cy5	640	450 – 700
LNP-LR	561	565 – 700

Supplementary Movie 1. 3D reconstruction of DNA localization, related to Fig. 1A
3D reconstruction of the cell in Fig. 1A showing localization of Cy-5 labelled plasmid DNA (pFL-*ssgB*; magenta) in an internal vesicle of *alpha* pIJ82-GFP (cytoplasmic eGFP; green) as generated using the 3D Viewer plugin in Fiji using standard settings (ImageJ).

Supplementary Movie 2. Uptake of Dextran-Texas Red by L-forms, related to Fig. 1E
Timelapse video of *alpha*-DivIVA-eGFP (green) incubated with 3 kDa Dextran-Texas Red (D-TR; magenta). Left: Brightfield. Right: Composite of green and magenta channels. Scale bar indicates 1 µm.

Supplementary Movie 3. 3D Reconstruction of vesicles in L-form cell, related to Fig. 3
3D segmentation volume rendering of vesicles of *alpha* pIJ82-GFP based on FIB-SEM Z-stack slices corresponding to Fig. 3H and Supplementary Fig. 6A. Colours indicate individual vesicles or vesicle complexes. The cell is depicted in grey in the 3D Volume Rendering.

Supplementary Movie 4. 3D Reconstruction of vesicles in L-form cell, related to Fig. 3
3D segmentation volume rendering of vesicles of *alpha* pIJ82-GFP based on FIB-SEM Z-stack slices corresponding to Fig. 3I – Q and Supplementary Fig. 6B – D. Colours indicate individual vesicles or vesicle complexes. The cell is depicted in grey in the 3D Volume Rendering.

Supplementary Movie 5. Timelapse of putative vesicle disruption, related to Supplementary Fig. 7
Timelapse of *alpha* pRed* expressing cytoplasmic mCherry, showing putative vesicle disruption between 01:00 to 01:15 h:min of incubation. The vesicle was present from the start of the incubation. Cells were incubated at 30 °C and imaged overnight using the Lionheart FX automated microscope. Images were taken every 15 min for 20 h. Left: Brightfield. Right: mCherry emission. See also Supplementary Fig. 7A.

Supplementary Movie 6. Timelapse of putative vesicle disruption, related to Supplementary Fig. 7
Timelapse of *alpha* pRed* expressing cytoplasmic mCherry, showing putative vesicle disruption between 13:30 to 13:45 h:min of incubation. The vesicle was present from the start of the incubation. Cells were incubated at 30 °C and imaged overnight using the Lionheart FX automated microscope. Images were taken every 15 min for 17.5 h. Left: Brightfield. Right: mCherry emission. See also Supplementary Fig. 7B.

Supplementary Movie 7. Timelapse of putative vesicle disruption, related to Supplementary Fig. 7
Timelapse of *alpha* pRed* expressing cytoplasmic mCherry, showing putative vesicle disruption between 17:15 to 17:30 h:min of incubation, after which the timelapse had ended. Note that the movie shows the incubation from 15 h onwards. The vesicle was present from the start of the incubation. Cells were incubated at 30 °C and imaged overnight using the Lionheart FX automated microscope. Images were taken every 15 min for 17.5 h. Left: Brightfield. Right: mCherry emission. See also Supplementary Fig. 7C.